Journal of Power Sources 196 (2011) 3810–3823

Contents lists available at ScienceDirect

Journal of Power Sources

journal homepage: www.elsevier.com/locate/jpowsour

Modeling of the Ballard-Mark-V proton exchange membrane fuel cell with power converters for applications in autonomous underwater vehicles☆

Chien-Hsing Lee*, Jian-Ting Yang

Department of Systems and Naval Mechatronic Engineering, National Cheng Kung, University, 1, University Rd., Tainan 701, Taiwan, ROC

ARTICLE INFO

Article history:
Received 21 November 2010
Received in revised form
10 December 2010
Accepted 10 December 2010
Available online 21 December 2010

Keywords:
Fuel cells
Autonomous underwater vehicles
Voltage-model control
dc–dc converters

ABSTRACT

This paper studies the transient response of the output voltages of a Ballard-Mark-V 35-cell 5 kW proton exchange membrane fuel cell (PEMFC) stack with power conversion for applications in autonomous underwater vehicles (AUVs) under load changes. Four types of pulse-width modulated (PWM) dc–dc power converters are employed to connect to the studied fuel cell in series for converting the unregulated fuel cell stack voltage into the desired voltage levels. The fuel cell model in this paper consists of the double-layer charging effect, gases diffusion in the electrodes, and the thermodynamic characteristic; PWM dc–dc converters are assumed to operate in continuous-conduction mode with a voltage-mode control compensator. The models of the study's fuel cell and PWM dc–dc converters have been implemented in a Matlab/SIMULINKTM environment. The results show that the output voltages of the studied PEMFC connected with PWM dc–dc converters during a load change are stable. Moreover, the model can predict the transient response of hydrogen/oxygen out flow rates and cathode and anode channel temperatures/pressures under sudden change in load current.

1. Introduction

Over the past few years, hydrogen production and fuel cell technologies have grown dramatically. Proton exchange membrane fuel cells (PEMFC) are one of the most promising fuel cell technologies that can be a candidate for both stationary and automotive applications [1]. The traditional energy source of underwater vehicles is based on the heat engine process of the Carnot cycle. It causes not only low conversion efficiency but also pollutions. Recently, an unmanned untethered submersible AUV-HM1 testbed developed by National Taiwan University has been powered by lead-acid batteries. However, the limited operating range detracts from the usages of them. In order to design a long-range underwater vehicle, the larger capacity of the lead-acid battery is needed but this will increase the weight and occupy most of the volume of the underwater vehicle. Thus, fuel cells coupled with an alternative reactant storage system may have tried to overcome these limitations while maintaining other benefits of an electrochemical power source [2–6].

Generally, the PEMFC has multiple advantages. It offers a quiet low temperature operating condition with only producing a clean byproduct—pure water and is stackable to provide a range of space options. Its disadvantage is that pure hydrogen and oxygen reactants must be carried. Thus, fuel storage is a key component for applying the PEMFC to underwater vehicles. For the PEMFC, pure hydrogen must be stored. Hydrogen can be stored as a gas, liquid, or in a hydride. Out of the three options researched, the hydride method is chosen for its proven safety and reliability advantages [4].

The purpose of this paper is to study the performance of the combined PEMFC and pulse-width modulated (PWM) dc–dc converters subject to a load change in autonomous underwater vehicles (AUVs). Although [7] has already described the PEMFC performance in the presence of transient effects, it did not use power converters to regulate the output voltage of the fuel-cell stack. In addition, [8] has built a nonlinear model of buck converters, and in [9–11] have mentioned to the use of boost converters to regulate the output voltage of the fuel-cell stack. Nevertheless, they have not yet shown the phenomenon that the load variations may affect the output voltage of the power converter.

2. Mathematical model of the PEMFC

This section describes a mathematical model for investigating the mass and energy dynamic interactions as well as the electrochemical reaction within a PEMFC [12,13]. As seen from Fig. 1, the hydrogen enters the anode channel, and diffuses through the anode diffusion layer toward the active catalyst layer, where the hydrogen

☆ This work was supported in part by the National Science Council, Taiwan, under Grant NSC 99-2221-E-006-227.

* Corresponding author. Tel.: +886 6 2757575x63539; fax: +886 6 2747019.
E-mail addresses: chienlee@mail.ncku.edu.tw (C.-H. Lee), p1696123@mail.ncku.edu.tw (J.-T. Yang).

0378-7753/$ – see front matter © 2010 Elsevier B.V. All rights reserved.
doi:10.1016/j.jpowsour.2010.12.049

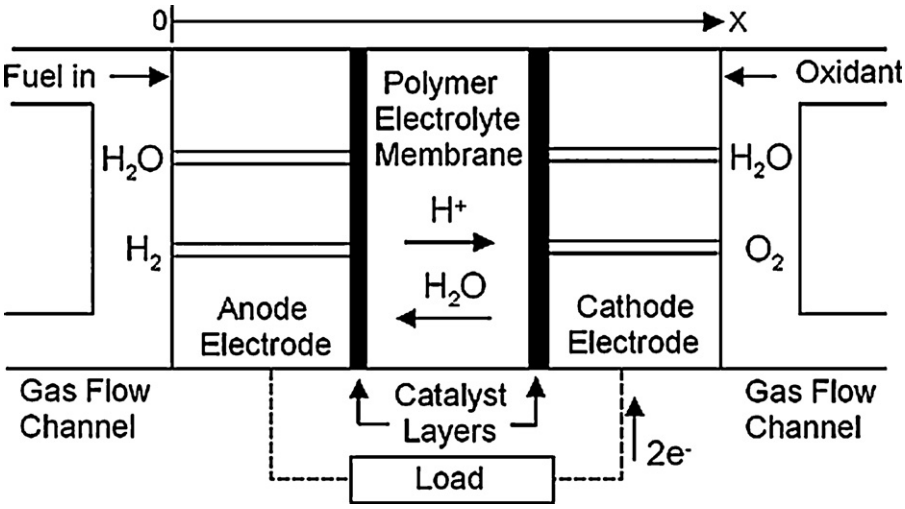

Fig. 1. Schematic diagram of a PEMFC.

dissociates into protons and electrons. The protons then travel from the anode catalyst to the cathode catalyst through a membrane. In the meantime, oxygen enters the cathode channel, part of which diffuse through the cathode diffusion layer to the active catalyst, where the oxygen dissociates and combines with protons and electrons to form water, while heat and current are generated. The heat produced during the reduction reaction process will warm up the fuel cell body that will affect the mass diffusion within the anode diffusion layer, cathode diffusion layer and membrane. Typically, the heat transfers to ambient and gas flow channels through convection and radiation. The resulting gas temperature variation will change the pressure and flow rate within the channels to affect the gas diffusion within the diffusion layers. All these dynamic interactions will have a direct effect on the fuel cell output voltage and current.

2.1. Relationship between mass and energy transfer using control volume approach

For an arbitrary control volume, a continuity equation in an integral form is given as [14]:

$$\frac{\partial}{\partial t}\iiint_{\text{C.V.}} \rho \, \mathrm{d}V + \oiint_{\text{C.S.}} \rho(\vec{V}\cdot\vec{n})\,\mathrm{d}A = 0 \tag{1}$$

and an energy equation in integral form is expressed by

$$\frac{\partial}{\partial t}\iiint_{\text{C.V.}} \rho e_t \, \mathrm{d}V + \oiint_{\text{C.S.}} \rho h(\vec{V}\cdot\vec{n})\,\mathrm{d}A = \frac{\mathrm{d}Q}{\mathrm{d}t} + \frac{\mathrm{d}W}{\mathrm{d}t} \tag{2}$$

where ρ is the material density within the control volume, $\vec{V}$ is the velocity vector of flow fluid, $\vec{n}$ is the unit vector normal to the control surface toward the outside, e_t is the specific internal energy, h is the specific enthalpy, Q is the heat added to the control volume, and W is the work done on the control volume. Since the gas flow velocity is usually low under fuel cell operating conditions, the kinetic and potential energies of the gases can be neglected in (2). Note that the anode channel control volume is defined to be the lumped volume from the anode inlet to the anode outlet. Similarly, the cathode channel control volume is defined at the cathode side. The membrane electrode assembly (MEA) and all other metal structures involved in the fuel cell will form the fuel cell body control volume. As for considering a fuel cell stack, the control volumes of the anode channel, cathode channel and fuel cell body will be the summation of corresponding control volumes of each single cell. In addition, the physical properties associated with the control volumes are assumed to be uniform.

2.1.1. Anode and cathode channels

Generally, air or oxygen is fed to the cathodic compartment while hydrogen is fed to the anodic one and the electrolyte performs both the functions of transferring H^+ from the anode to the cathode and reactant separation. Note that pure hydrogen and oxygen are served as the fuel and oxidant gases for underwater applications, respectively. Thus, the first term in (1) becomes the mass change rate of the respective gases for the control volumes corresponding to the anode and cathode channels. The second term in (1) is the mass flow rate through the surface of the control volumes.

For the anode channel, the hydrogen mass change rate is written to be [12,13]:

$$\frac{\partial}{\partial t}\iiint_{\text{C.V.}} \rho_{\text{H}_2} \, \mathrm{d}V = \frac{\mathrm{d}m_{\text{H}_2}}{\mathrm{d}t} \tag{3}$$

and the mass flow rate through the surface of the control volumes is expressed by

$$-\oiint_{\text{C.S.}} \rho_{\text{H}_2}(\vec{V}\cdot\vec{n})\,\mathrm{d}A = W_{\text{H}_2,\text{in}} - W_{\text{H}_2,\text{out}} - W_{\text{H}_2,\text{used}} \tag{4}$$

where $W_{\text{H}_2,\text{in}}$ and $W_{\text{H}_2,\text{out}}$ are the inlet and outlet mass flow rates, respectively. They are as functions of the hydrogen source pressure, the pressure within the anode control volume and ambient pressure. With the macroscopic level dynamic behavior of the fuel cell, the inlet and outlet mass flow rates can be simplified by using the traditional nozzle flow rate equation which are written to be [12]:

$$W_{\text{H}_2,\text{in}} = k_{\text{an,in}}(p_{\text{an},s} - p_{\text{an}}) \tag{5}$$

$$W_{\text{H}_2,\text{out}} = k_{\text{an,out}}(p_{\text{an}} - p_{\text{atm}}) \tag{6}$$

where $k_{\text{an,in}}$ and $k_{\text{an,out}}$ are the inlet and outlet mass flow rate coefficients; $p_{\text{an,s}}$, p_{an} and p_{atm} are the hydrogen source pressure, the pressure within the anode control volume and ambient pressure, respectively. In addition, the consumed mass flow rate of hydrogen is

$$W_{\text{H}_2,\text{used}} = M_{\text{H}_2}\frac{N_{\text{cell}}I}{2F} \tag{7}$$

where I denotes the current, N_{cell} is the number of cells in a stack; F and M_{H_2} are Faraday's constant and hydrogen's mole mass, respectively. Thus, the hydrogen mass transport rate through the

anode channel control surface becomes:

$$\frac{dm_{H_2}}{dt} = k_{an,in}(p_{an,s} - p_{an}) - k_{an,out}(p_{an} - p_{atm}) - M_{H_2}\frac{N_{cell}I}{2F} \quad (8)$$

Furthermore, the energy equation of (2) can be applied to the anode in a similar manner. The first term on the left-hand side of (2) represents the internal energy change rate of hydrogen within the anode channel control volume which is given as [12,13]:

$$\frac{\partial}{\partial t}\iiint_{C.V.} \rho_{H_2} e_t \, dV = \frac{d(m_{H_2} c_{v,H_2} T_{an})}{dt} \quad (9)$$

where c_{v,H_2} is the specific heat of hydrogen at constant volume and T_{an} is the hydrogen temperature within the anode channel control volume. The second term on the left-hand side of (2) is the heat transfer rate due to the mass transport through the control surface which is given as:

$$-\oiint_{C.S.} \rho_{H_2} h_{H_2} (\vec{V}\cdot\vec{n})\, dA = W_{H_2,in} h_{H_2,in} - W_{H_2,out} h_{H_2,out} - W_{H_2,used} h_{H_2,used} \quad (10)$$

where $h_{H_2,in}$ and $h_{H_2,out}$ are the inlet and outlet specific enthalpy hydrogen, respectively; $h_{H_2,used}$ is the specific enthalpy of consumed hydrogen. Since the temperature of a PEMFC body is relatively moderate, the radiation effect can be neglected. Based on Newton's cooling law for governing the convection heat transfer mechanism, the convection heat transfer from the cell body to the anode channel can be described as [12,13]:

$$\frac{dQ}{dt} = \dot{Q}_{conv,an} = h_{conv,an} A_{conv,an}\, \Delta T = k_{conv,an}(T_{body} - T_{an}) \quad (11)$$

where $h_{conv,an}A_{conv,an} = k_{conv,an}$, $h_{conv,an}$ is the convection heat transfer coefficient at the anode; $A_{conv,an}$ is the surface area of hest convection at the anode. Note that the work done on the control volume (i.e., dW/dt) disappears since the viscous normal stresses at the inlet, outlet and electrode interface of mass diffusion are neglected. Thus, the energy equation for the anode becomes:

$$\frac{d(m_{H_2} c_{v,H_2} T_{an})}{dt} = k_{conv,an}(T_{body} - T_{an}) + k_{an,in}(p_{an,s} - p_{an}) c_{p,H_2}(T_{an,in} - T_0) - k_{an,out}(p_{an} - p_{atm}) c_{p,H_2}(T_{an} - T_0) - \frac{N_{cell}I}{2F} M_{H_2} c_{p,H_2}(T_{an} - T_0) \quad (12)$$

where $T_{an,in}$ and T_0 are the flow-in hydrogen temperature and the reference temperature (i.e., 298.15 K), respectively. $c_{p,H}$ is the average specific heat of hydrogen.

For the cathode channel, similar equations can be derived by replacing the relevant subscripts by "ca" (cathode) and "O_2" (oxygen). The following equations are parallel to those given in (3) and (4) and (8)–(12):

$$\frac{\partial}{\partial t}\iiint_{C.V.} \rho_{O_2}\, dV = \frac{dm_{O_2}}{dt} \quad (13)$$

$$-\oiint_{C.S.} \rho_{O_2}(\vec{V}\cdot\vec{n})\, dA = W_{O_2,in} - W_{O_2,out} - W_{O_2,used} \quad (14)$$

$$\frac{dm_{O_2}}{dt} = k_{ca,in}(p_{ca,s} - p_{ca}) - k_{ca,out}(p_{ca} - p_{atm}) - M_{O_2}\frac{N_{cell}I}{4F} \quad (15)$$

$$\frac{\partial}{\partial t}\iiint_{C.V.} \rho_{O_2} e_t \cdot dV = \frac{d(m_{O_2} c_{v,O_2} T_{ca})}{dt} \quad (16)$$

$$-\oiint_{C.S.} \rho_{O_2} h_{O_2}(\vec{V}\cdot\vec{n})\cdot dA = W_{O_2,in} h_{O_2,in} - W_{O_2,out} h_{O_2,out} - W_{O_2,used} h_{O_2,used} \quad (17)$$

$$\frac{dQ}{dt} = \dot{Q}_{conv,ca} = k_{conv,ca}(T_{body} - T_{ca}) \quad (18)$$

$$\frac{d(m_{O_2} c_{v,O_2} T_{ca})}{dt} = k_{conv,ca}(T_{body} - T_{ca}) + k_{ca,in}(p_{ca,s} - p_{ca}) c_{p,O_2}(T_{ca,in} - T_0) - k_{ca,out}(p_{ca} - p_{atm}) c_{p,O_2}(T_{ca} - T_0) - \frac{N_{cell}I}{4F} M_{O_2} c_{p,O_2}(T_{ca} - T_0) \quad (19)$$

2.1.2. Cell body

The continuity equation for the cell body control volume is only concerned with the species' conservation of electrochemical reaction. That is, water is formed through the electrochemical reaction by consuming hydrogen and oxygen. Since most parts of the cell body are composed of metal structures, gas diffusion and water produced have little effect on the total mass change of cell body. Thus, we will have [12,13]:

$$\frac{\partial}{\partial t}\iiint_{C.V.} \rho_{body}\, dV = 0 \quad (20)$$

and the mass transport rate through the cell body control surface (Membrane Electrode Assembly, MEA) is

$$-\oiint_{C.S.} \rho_{body}(\vec{V}\cdot\vec{n})\, dA = W_{H_2,used} + W_{O_2,used} - W_{H_2O} \quad (21)$$

Note that the above equation includes the gas diffusion through the electrodes and water formed by electrochemical reactions.

Now let us consider the energy equation for the cell body control volume. The internal energy change rate of cell body is given as [12,13]:

$$\frac{\partial}{\partial t}\iiint_{C.V.} \rho_{body} e_t\, dV = m_{body} c_{p,body}\frac{dT_{body}}{dt} \quad (22)$$

and the heat transfer rate due to the mass transport through the control surface is given as:

$$-\oiint_{C.S.} \rho_{body} h_{body}(\vec{V}\cdot\vec{n})\, dA = W_{H_2,used} h_{H_2,used} + W_{O_2,used} h_{O_2,used} - W_{H_2O} h_{H_2O} \quad (23)$$

where $c_{p,body}$ is the average specific heat of the cell body. In addition, several heat transfer effects are involved in the term dQ/dt, which include the heat added to the cell body through the electrochemical reaction as well as the heat transferred to the ambient and the channels via convection. Thus, we have [12,13]:

$$\frac{dQ}{dt} = \dot{Q}_{conv,an} + \dot{Q}_{conv,ca} + \dot{Q}_{conv,amb} + \Delta H_{R,T}\oiint_{electrode} \rho_{H_2}(\vec{V}\cdot\vec{n})\, dA \quad (24)$$

where $Q_{conv,an}$ is the heat convection between the cell body and the anode channel, $Q_{conv,ca}$ is the heat convection between the cell body and the cathode channel, $Q_{conv,amb}$ is the heat convection between the cell body and the ambient, and $\Delta H_{R,T}$ is the lower heating value of the fuel. All the heat convection terms here are assumed to comply with Newton's cooling law. For the cell body, the term dW/dt is the electric power converted from electrochemical reaction, i.e.:

$$\frac{dW}{dt} = -V'_{stack} I \quad (25)$$

where V'_{stack} denotes the stack voltage. Thus, the heat added to and the work done on the cell body control volume is then characterized as:

$$\frac{dQ}{dt} + \frac{dW}{dt} = k_{conv,an}(T_{an} - T_{body}) + k_{conv,ca}(T_{ca} - T_{body}) + k_{conv,amb}(T_{amb} - T_{body}) + \Delta H_{R,T}\frac{N_{cell}I}{2F} M_{H_2} - V'_{stack} I \quad (26)$$

Note that the first three terms at right-hand side are the effects of the convection heat transfer from the surrounding structures, the fourth term on the right-hand side is the heat produced by the electrochemical, and the last term is the converted electric power. Finally, the energy equation for the cell body will become

$$m_{body}C_{p,body}\frac{dT_{body}}{dt} = \Delta H_{R,T}\frac{N_{cell}I}{2F}M_{H_2} - V'_{stack}I + k_{conv,an}(T_{an}-T_{body}) + k_{conv,ca}(T_{ca}-T_{body}) + k_{conv,amb}(T_{amb}-T_{body}) + W_{H_2,used}c_{p,H_2}(T_{an}-T_{body}) + W_{O_2,used}c_{p,O_2}(T_{ca}-T_{body}) - W_{H_2O}c_{p,H_2O}(T_{ca}-T_{body}) \quad (27)$$

2.2. Reactant gases diffusion in the electrodes

To simply the mathematical model of the PEMFC, the following assumptions are made in this paper [15–21]:

(1) One-dimensional treatment.
(2) Ideal and uniformly distributed gases.
(3) Constant pressures in the fuel-cell gas flow channels.
(4) The fuel is humidified H_2 and the oxidant is humidified O_2. Assume the effective anode water vapor pressure is 50% of the saturated vapor pressure while the effective cathode water pressure is 100%.
(5) The reaction gases are pure hydrogen and oxygen.
(6) Parameters for individual cells can be lumped together to represent a fuel-cell stack.
(7) As mentioned in [20], the saturated vapor pressure $\rho^{sat}_{H_2O}$ is a function of the operating temperature of the PEMFC and is written to be

$$\log(\rho^{sat}_{H_2O}) = 2.95\times10^{-2}(T_{body}-273.15) - 9.18\times10^{-5}(T_{body}-273.15)^2 + 1.44\times10^{-7}(T_{body}-273.15)^3 - 2.18 \quad (28)$$

In order to calculate the PEMFC output voltage, the effective partial pressures of H_2 and O_2 need to be determined. In a gas mixture consisting of N species, the diffusion of component i through the porous electrodes can be described using Stefan-Maxwell equations as written to be [21]:

$$\nabla X_i = \sum_{j=1}^{n}\frac{RT_{body}}{PD_{i,j}}(X_iN_j - X_jN_i), \quad i = 1,2,\ldots,n \quad (29)$$

In the one-dimensional transport process along the X-axis as shown in Fig. 1, the effective mole fraction of water at the anode catalyst interface is given as:

$$X_{H_2O} = X^{channel}_{H_2O}\exp\left(\frac{RT_{body}J\ell_{ac}}{2FP_{an}D_{H_2O,H_2}}\right) \quad (30)$$

Since $X_{H_2} + X_{H_2O} = 1$, the effective partial pressure of H_2 at the interface is

$$\rho_{H_2} = (1-X_{H_2O})\frac{\rho^{sat}_{H_2O}}{X_{H_2O}} \quad (31)$$

According to assumption 4 mentioned above, the effective anode water vapor pressure is 50% of the saturated vapor pressure. Thus, the effective partial pressure of H_2 by combining (30) and (31) yields:

$$\rho_{H_2} = 0.5\rho^{sat}_{H_2O}\left[\frac{1}{X^{channel}_{H_2O}\exp((RT_{body}J\ell_{ac})/2FP_{an}D_{H_2O,H_2})} - 1\right] \quad (32)$$

Similar to the analysis for the anode, the effective mole fraction of water at the cathode catalyst interface can be found as:

$$X_{H_2O} = X^{channel}_{H_2O}\exp\left(\frac{RT_{body}J\ell_{cc}}{4FP_{ca}D_{H_2O,O_2}}\right) \quad (33)$$

As the partial pressure of water vapor in the cathode is fixed at the saturation level, the partial pressure of O_2 at the interface is

$$\rho_{O_2} = (1-X_{H_2O})\frac{\rho^{sat}_{H_2O}}{X_{H_2O}} \quad (34)$$

Also, the effective cathode water vapor pressure equals the saturated vapor pressure based on assumption 4. Thus, the effective partial pressure of O_2 by combining (33) and (34) yields:

$$\rho_{O_2} = \rho^{sat}_{H_2O}\left[\frac{1}{X^{channel}_{H_2O}\exp((RT_{body}J\ell_{cc})/4FP_{ca}D_{H_2O,O_2})} - 1\right] \quad (35)$$

Using the appropriate critical values and constants for a water/oxygen mixture, (32) and (35) finally becomes:

$$\rho_{H_2} = 0.5\rho^{sat}_{H_2O}\left[\frac{1}{X^{channel}_{H_2O}\exp((1.653J)/T^{1.334}_{body})} - 1\right] \quad (36)$$

$$\rho_{O_2} = \rho^{sat}_{H_2O}\left[\frac{1}{X^{channel}_{H_2O}\exp((4.192J)/T^{1.334}_{body})} - 1\right] \quad (37)$$

where (36) and (37) will be used in the Nernst equation to find the fuel-cell output voltage.

2.3. Output voltage of the fuel-cell stack

The total output voltage of a fuel-cell stack is a function of stack current, cathode pressure, reactant partial pressures, fuel cell temperature, membrane humidity, etc. Since the fuel-cell stack is comprised of multiple fuel cells connected in series, the stack voltage V_{stack} is calculated by multiplying the cell voltage V_{cell} by a number of cells N_{cell} in the stack, which is written as:

$$V_{stack} = N_{cell}\cdot V_{cell} \quad (38)$$

The output voltage of a single fuel cell is defined by the sum of three voltage terms: the thermodynamic potential E_{nernst}, the activation overvoltage V_{act}, and the ohmic overvoltage V_{ohm} as repeated below [15–19]:

$$V_{cell} = E_{nernst} - V_{act} - V_{ohm} \quad (39)$$

where

$$E_{nernst} = E_0 - 0.85\times10^{-3}(T_{body}-298.15) + \frac{RT_{body}}{2F}\ell n[\rho_{H_2}\cdot(\rho_{O_2})^{0.5}] \quad (40)$$

$$V_{act} = -\{\xi_1 + \xi_2T_{body} + \xi_3T_{body}[\ell n(C_{O_2})] + \xi_4T_{body}\ell n(I)\} \quad (41)$$

$$\xi_2 = 0.00286 + 0.0002\ell n(A_{cell}) + 4.3\times10^{-5}\ell n(C_{H_2}) \quad (42)$$

$$C_{O_2} = 1.97\times10^{-7}\rho_{O_2}\exp\left(\frac{498}{T_{body}}\right) \quad (43)$$

$$C_{H_2} = 9.174\times10^{-7}\rho_{H_2}\exp\left(\frac{-77}{T_{body}}\right) \quad (44)$$

$$V_{ohm} = I\cdot R_{int} \quad (45)$$

$$R_{int} = \frac{r_{mem}t_{mem}}{A_{cell}} \quad (46)$$

$$r_{\text{mem}} = \frac{181.6[1 + 0.03J + 0.062(T_{\text{body}}/303)^2 J^{2.5}]}{[\lambda - 0.634 - 3J]\exp[4.18((T_{\text{body}} - 303)/T_{\text{body}})]} \quad (47)$$

Note that the two overvoltage terms in (39) are both negative and represent nonideal fuel-cell reaction conditions. From an electrical/power-electronics standpoint, a fuel cell is almost a nonlinear current-dependent voltage source. While this functional relationship varies somewhat with different fuel cells (e.g., solid oxide fuel cell, SOFC), [22–24] have outlined more detailed work on planar SOFC.

2.4. Double-layer charging effect

The double layer charging capacitance may affect the activation overvoltage term in (39). This results in a first-order model where a sudden change in cell current is associated with a slower variation in output voltage [17,19]. An electrical circuit model is generally used to illustrate this capacitive effect [17]. For a given cell current, the activation voltage drop can be considered across an activation resistance R_{act}. Since the activation voltage term V_{act} introduced in (41) is negative, the derivation of a positive term V_{d} is required. The first-order dynamics of the activation overvoltage are described by the equations as follows [17,19]:

$$R_{\text{act}} = \frac{V_{\text{act}}}{I} \quad (48)$$

$$\frac{dV_{\text{d}}}{dt} = \frac{I}{C_{\text{dl}}} - \frac{V_{\text{d}}}{R_{\text{act}} C_{\text{dl}}} \quad (49)$$

If the double-layer charging effect is integrated into the modeling by using V_{d} instead of V_{act}, to calculate V'_{stack}, the fuel-cell output voltage now turns out to be:

$$V'_{\text{stack}} = N_{\text{cell}}(E_{\text{nernst}} - V_{\text{d}} - V_{\text{ohm}}) \quad (50)$$

Note that the dynamical model for PEMFC electrochemistry described in this section is based on a generalized empirical set of equations. Thus, by identifying appropriate parameters (i.e., number of cells, cell area, membrane thickness, etc.), fuel cells with varying sizes, structures, and materials can be modeled, and the relevant dynamics can be studied [17,19]. Table 1 lists the related parameters used to model the PEMFC in this paper.

Table 1
Parameters of the Ballard-Mark-V PEMFC.

Symbol	Parameter	Value	Unit
$k_{\text{an,in}}$	Upstream nozzle coefficient of a node channel	4.2×10^{-5}	kg (s atm)$^{-1}$
$k_{\text{an,out}}$	Downstream nozzle coefficient of a node channel	4.2×10^{-6}	kg (s atm)$^{-1}$
$p_{\text{an,s}}$	Pressure of anode	35	psig
$T_{\text{an,in}}$	Upstream hydrogen temperature of anode channel	296.5	K
c_{v,H_2}	Specific heat of hydrogen at constant volume	10,124.71	J (kg K)$^{-1}$
$c_{p,\ 2}$	Specific heat of hydrogen at constant pressure	14,209	J (kg K)$^{-1}$
V_{an}	Volume of the anode channel	0.005	m^3
$k_{\text{conv,an}}$	Heat convection coefficient between the cell body and the anode channel	2	W K^{-1}
R_{H_2}	Gas constant of hydrogen	4071.1×10^{-5}	atm m^3 (kg K)$^{-1}$
M_{H_2}	Molecular mass of hydrogen	2×10^{-3}	kg mol^{-1}
$k_{\text{ca,in}}$	Upstream nozzle coefficient of a cathode channel	1.8×10^{-3}	kg (s atm)$^{-1}$
$k_{\text{ca,out}}$	Downstream nozzle coefficient of a cathode channel	2.71×10^{-4}	kg (s atm)$^{-1}$
$p_{\text{ca,s}}$	Pressure of cathode	35	psig
$T_{\text{ca,in}}$	Upstream hydrogen temperature of cathode channel	296.5	K
c_{v,O_2}	Specific heat of oxygen at constant volume	662.2	J (kg K)$^{-1}$
c_{p,O_2}	Specific heat of oxygen at constant pressure	922	J (kg K)$^{-1}$
V_{ca}	Volume of the cathode channel	0.01	m^3
$k_{\text{conv,ca}}$	Heat convection coefficient between the cell body and the cathode channel	10	W K^{-1}
R_{O_2}	Gas constant of oxygen	262.68×10^{-5}	atm m^3 (kg K)$^{-1}$
M_{O_2}	Molecular mass of oxygen	32×10^{-3}	kg mol^{-1}
$k_{\text{conv,amb}}$	Heat convection coefficient between the cell body and the ambient	17	W K^{-1}
$m_{\text{body}}C_{\text{p,body}}$	Product of mass and the average specific heat of the cell body	3.5×10^4	J K^{-1}
p_{atm}	Ambient pressure	1	atm
T_{amb}	Ambient temperature	296.5	K
$c_{p,\text{H}_2\text{O}}$	Specific hest of water at constant pressure	2186	J (kg K)$^{-1}$
$\Delta H_{R,T}$	Lower heating value	1.196×10^8	J
λ	Membrane resistivity parameter	12.5	
ξ_1	Coefficients of activation over voltage	−0.948	–
ξ_3	Coefficients of activation over voltage	-1.93×10^{-4}	–
ξ_4	Coefficients of activation over voltage	7.6×10^{-5}	–
C_{dl}	Double layer capacitance	0.035×232	F
t_{mem}	Membrane thickness	1.78×10^{-2}	cm
E_0	Reference potential at unity activity	1.229	V
R	University gas constant	8.314	J (mol K)$^{-1}$
N_{cell}	Number of cells in the fuel-cell stack	35	–
A_{cell}	Fuel cell active area	232	cm^2
F	Faraday constant	96,485	C mol^{-1}

3. Design of DC/DC power converters

For the designed AUV, there are four desired voltage levels including 5-, 12-, 24- and 48-V_{dc} in response to changes in the output load and the PEMFC output voltage. To achieve this, a negative feedback control system is used where the converter output is compared with its reference value. The compensator produces the control voltage, which is used to adjust the duty cycle of the switch in the converter [25–27]. This section describes the design of the compensation networks.

Assume that all power switches and diodes are ideal elements, and the circuit operates in continuous-conduction mode (CCM). Additionally, an equivalent series resistance r_C associated with the capacitor and a series parasitic resistance r_L associated with the inductor including the converter equivalent circuit as shown in Fig. 2 are added to increase the simulation accuracy [28–30]. As seen from Fig. 2, the minimum values of the inductances and capacitances in the converter can be obtained from the input voltage, load size, switching frequency, and output voltage. These values are used as a reference to design the electrical elements of power converters. Since the converter itself is a part of the control loop, the design of such control processes requires a knowledge of the small-signal characteristics of the converter. Based on the gain and phase margin of the open-loop control-to-output transfer function of the converter, the compensator is then utilized to mitigate steady-state errors. As a result, the stable output voltage can be obtained from this process.

3.1. Procedure and criterion of compensator design

The procedure of compensator design is simply described as follows:

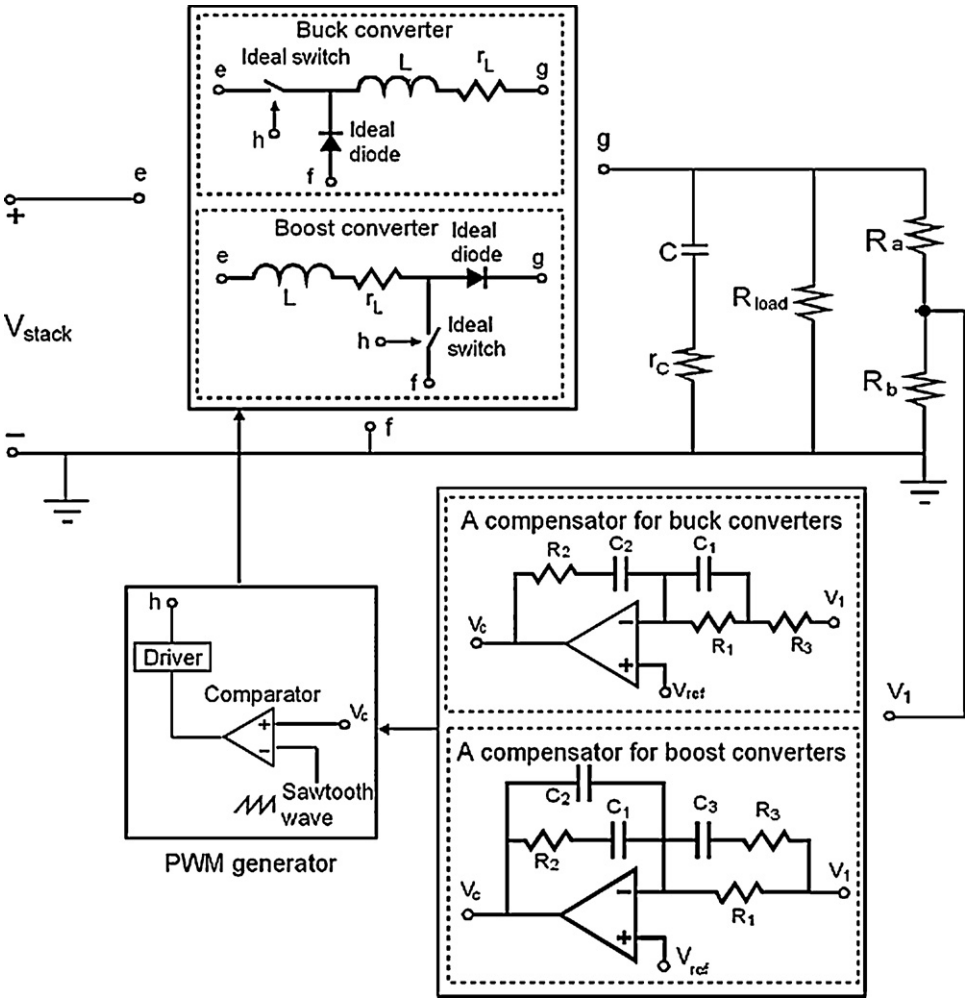

Fig. 2. Schematic diagram of the designed buck or boost converter.

(1) simulating the frequency response of the open-loop control-to-output transfer function of the converter,
(2) setting the gain crossover frequency for the converters and using this frequency to feedback the gain of the compensation circuit,
(3) selecting the compensator type as shown in Fig. 2 and designing the electrical elements of the compensation circuit, and
(4) simulating small-signal analysis of the frequency response of the closed-loop control-to-output transfer function of the converter.

As for the criterion of compensator design, it includes the following.

(1) The large dc gain is required to decrease the steady state error.
(2) The small gain switching frequency is required to suppress the noise produced during the switching.
(3) The gain crossover frequency of the converter is selected to be between 1/6 and 1/10 of the gain switching frequency.
(4) The phase and gain margins are suggested to be 45–60° and 6–20 dB, respectively.

3.2. Frequency response analysis

As for the designed buck converters, the slope of the frequency response of the open-loop control-to-output transfer function of the converter at the first corner is $-40\,\mathrm{dB\,dec^{-1}}$ because the two poles generated from the LC filter fall close to each other. Moreover, due to the equivalent series resistance associated with a capacitor, a zero occurs there at high frequency, resulting in the slope of $-20\,\mathrm{dB\,dec^{-1}}$. As for the designed boost converter, it not only has the characteristics of the frequency response of the designed buck converter but also has a right-half-plane zero. Based on the Bode diagram (i.e., gain and phase plots) for the open-loop control-to-output transfer function, one can select the compensator type as shown in Fig. 2, corner frequency, and gain curve. The values of electrical elements used in the compensation circuit are listed in Table 2 and the close-loop simulation circuit with the compensator for the designed buck and boost converters is shown in Fig. 2.

4. SIMULINK block diagrams

The mathematical expressions for the fuel-cell system and power converters were simulated in the Matlab/SIMULINK™ environment. A block diagram for building a dynamic model of PEMFC and power converters is given in Fig. 3. In this block diagram, the input quantities are anode and cathode pressures (P_{an} and P_{ca}) and operating temperature of the fuel cell (T_{op}). Additionally, mass diffusion equations are used to calculate the effective partial pressures of H_2 and O_2. Then, the Nernst equation is employed to determine the internal potential of the fuel cell. The ohmic voltage drop and activation voltage drop together with the double-layer charging

Table 2
Values of electrical elements in the circuits of the compensators and converters.

Parameters	Converters with the output voltage of			
	48 V	24 V	12 V	5 V
V_{stack}	20–40 V	24–40 V	20–40 V	20–40 V
f_s	50 kHz	50 kHz	50 kHz	50 kHz
L	10 μH	37.5 μH	20 μH	230 μH
r_L	10 mΩ	10 mΩ	10 mΩ	10 mΩ
C	1.6 mF	70 μF	600 μF	100 μF
r_c	10 mΩ	10 mΩ	10 mΩ	10 mΩ
R_{load}	8.2–1.37 Ω	24–3.84 Ω	2.4–0.384 Ω	25–4 Ω
R_1	37.3 kΩ	14.5 kΩ	3.55 kΩ	37.8 kΩ
R_2	316 kΩ	21.4 kΩ	15 kΩ	69.5 kΩ
R_3	1 kΩ	100 Ω	100 Ω	100 Ω
C_1	1.88 nF	4.8 nF	61.7 nF	8 nF
C_2	168 pF	7 nF	14.6 nF	4.36 nF
C_3	15.6 nF	–	–	–

effect are applied to determine the output voltage of a single fuel cell.

In Matlab/SIMULINK™ a set of equations can be grouped and are called subsystems. Detailed of these subsystems are given in Figs. 4–7. The PEMFC subsystem using the block diagram mentioned in Fig. 3 is shown in Fig. 4. The subsystem of reactant gases diffusion in the electrodes given in Fig. 5 employs (28)–(37) and calculates hydrogen/oxygen partial pressures. The subsystem of electrochemistry for Ballard-Mark-V PEMFC employs (38)–(48) using the parameters in Table 2 as shown in Fig. 6. It takes hydrogen/oxygen partial pressures, cell current, and temperatures as inputs and calculates the cell voltage. A gain at the terminal of the subsystem multiplies this output by the number of cells inside one stack. The subsystem of mass and energy transfer at the anode, cathode and cell body for Ballard-Mark-V PEMFC using the control volume approach employs (12), (19) and (27) with the parameters listed in Table 1 as shown in Fig. 7.

As for the power converter subsystem, it includes the circuits of power converters and compensators with voltage feedback control. Based on the electrical loads of the AUV, four converters are designed to obtain 5-, 12-, 24- and 48-V_{dc} output, and compensators are designed to regulate these dc voltages in the presence of transients. In Matlab/SIMULINK™ a model of the compensator circuit with voltage feedback control is built based on the references [31,32]. To limit the paper length, Fig. 8 only shows the model of the output voltage of 24V dc–dc converter. As seen from Fig. 8, the repeating sequence block is used to generate the sawtooth waveform, and the relay in discontinuities blockset is used to simulate the comparator. If the difference between the compensating signal and the sawtooth signal is positive, the switch is open and the output value is one; if the difference between the compensating signal and the sawtooth signal is negative, the switch is closed and the output value is zero.

5. Simulations results

5.1. Effects of operating conditions on cell performance of PEMFC

Fig. 9 shows the effects of using air or pure oxygen as the oxidant on the output voltage and output power for Ballard-Mark-V PEMFC. As seen from Fig. 9, the output voltage and output power using pure oxygen as the oxidant are higher than those obtained for the air. Due to the low operating temperature of the Ballard-Mark-V PEMFC, an increase in the operating temperature may result in a better cell performance because of a higher efficiency of the electrochemical reaction. Fig. 10 shows the output voltages of the studied fuel cell under different operating conditions of temperature and pressure. As seen from Fig. 10, a linear increase in the output voltage with increasing the operating temperature and pressure has been observed in a high current density range. In general, the operating temperature of the studied fuel cell is limited to approximately 80 °C, and both the anode and the cathode sides operating pressures are from 1 to 3 atm. As a result, due to the limitations of the underwater environment, the PEMFC uses pure hydrogen and pure oxygen as fuel in this study. Assuming the pressures of oxygen and hydrogen in the inlet gas are operated at 3 atm with the temperature at approximately 70 °C.

5.2. Simulation of PEMFC subsystem

Fig. 11 shows the total output voltage and output power for Ballard-Mark-V 35-cell 5-kW PEMFC based on the parameters mentioned in Table 2. As seen from Fig. 11, the sharp voltage drop at low currents is caused by an activation overvoltage, and the linear drop at intermediate currents is due to an ohmic overvoltage. Moreover, the maximum output power occurring at the load current of 239 A is about 3943 W, and the corresponding output voltage is about 16.5 V.

Since the loads of the designed AUV as listed in Table 3 are below 2 kW, the maximum output current of the studied fuel cell is computed to be about 78 A, and its corresponding output is ranged from 27 V to 40 V. Fig. 12 shows the output voltage and output current of Ballard-Mark-V 35-cell 5 kW PEMFC at a power output between 0.3 kW and 2 kW. As seen from Fig. 12, the PEMFC output voltage is not stable due to the polarization losses (i.e., activation and ohmic overvoltages). Thus, PWM dc–dc converters (i.e., three buck converters and one boost converter) are connected to the PEMFC output for converting unregulated dc voltage into four desired voltage levels. Note that PWM dc–dc converters are designed to operate under

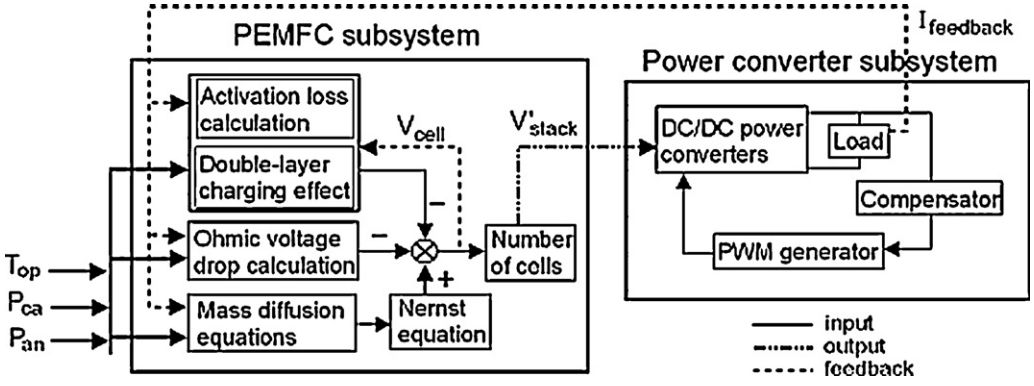

Fig. 3. Diagram of building the models of a PEMFC and dc–dc power converters.

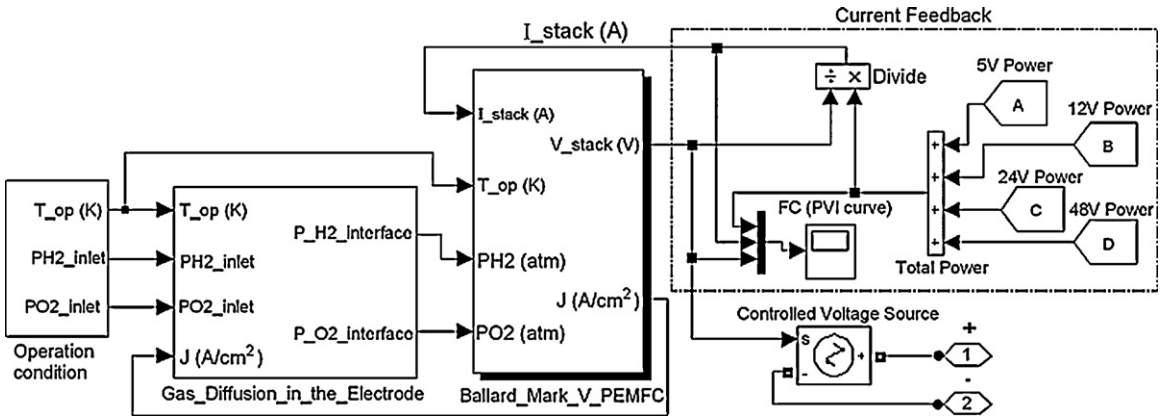

Fig. 4. SIMULINK block diagram of the Ballard-Mark-V PEMFC subsystem.

overloads and light load. The light-load, full-load, and overload conditions are defined to be 20%, 100% and 120% of the maximum rated power of the designed AUV as listed in Table 4, respectively.

For the purpose of simulation, no loss of energy is assumed for converting an input energy of Ballard-Mark-V 35-cell 5-kW PEMFC into an output power. The output power and output voltage of the studied fuel cell during a load change from full load to light load for all four buses of voltages are shown in Figs. 13 and 14. As seen from Fig. 13, the total output power of the studied fuel cell varies from 1841 W to 370 W as a load change occurs at 4 s during a simulation time of 8 s. As seen from Fig. 14, the output voltage and output current of the studied fuel cell are 29.3 V and 63.1 A at full load condition, respectively. However, the output voltage and output current of the studied fuel cell are 32.5 V and 11.4 A at light load condition, respectively.

5.3. Simulation of PWM dc–dc power converter subsystem

As for the designed AUV, four PWM dc–dc converters with the compensation network using voltage-model control are connected to the output of the studied fuel cell for converting unregulated

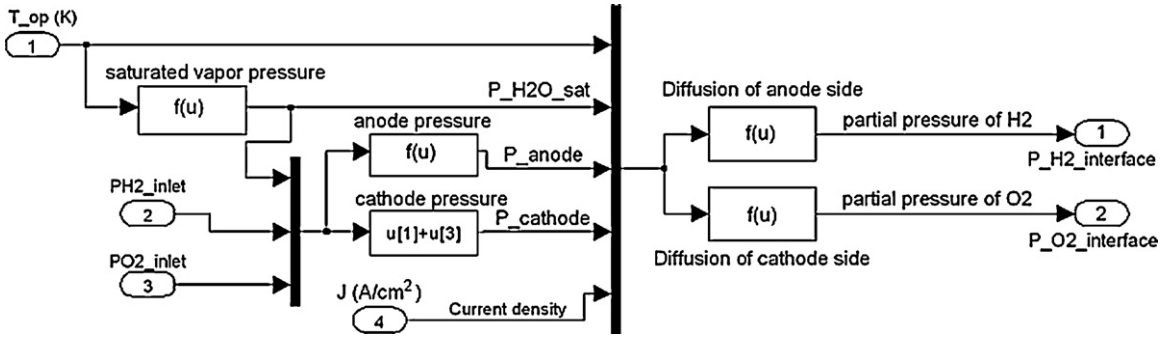

Fig. 5. SIMULINK block diagram of reactant gases diffusion in the electrodes.

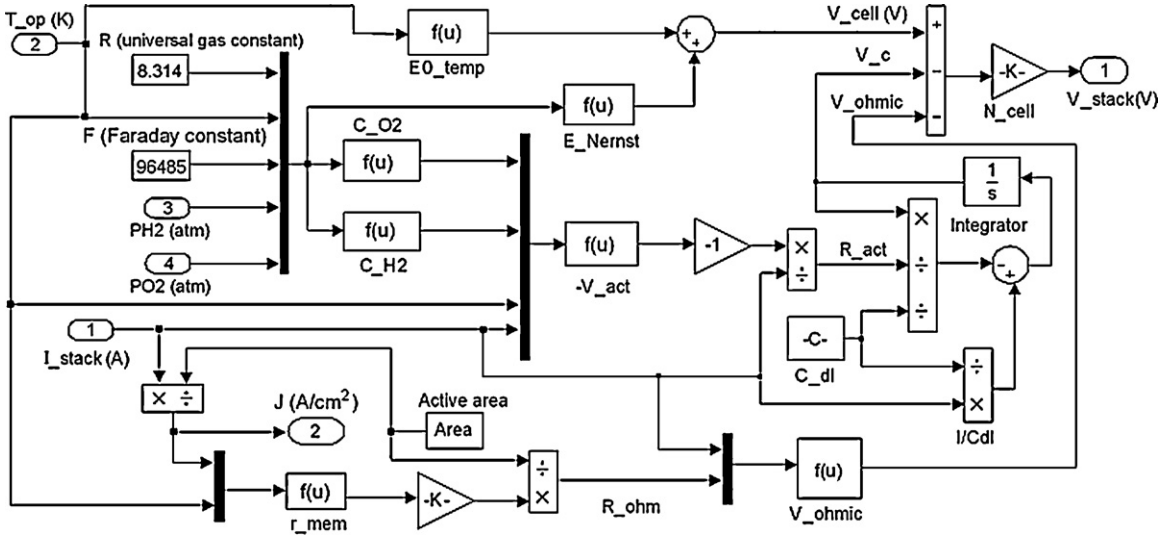

Fig. 6. SIMULINK block diagram of the electrochemistry subsystem of Ballard-Mark-V PEMFC.

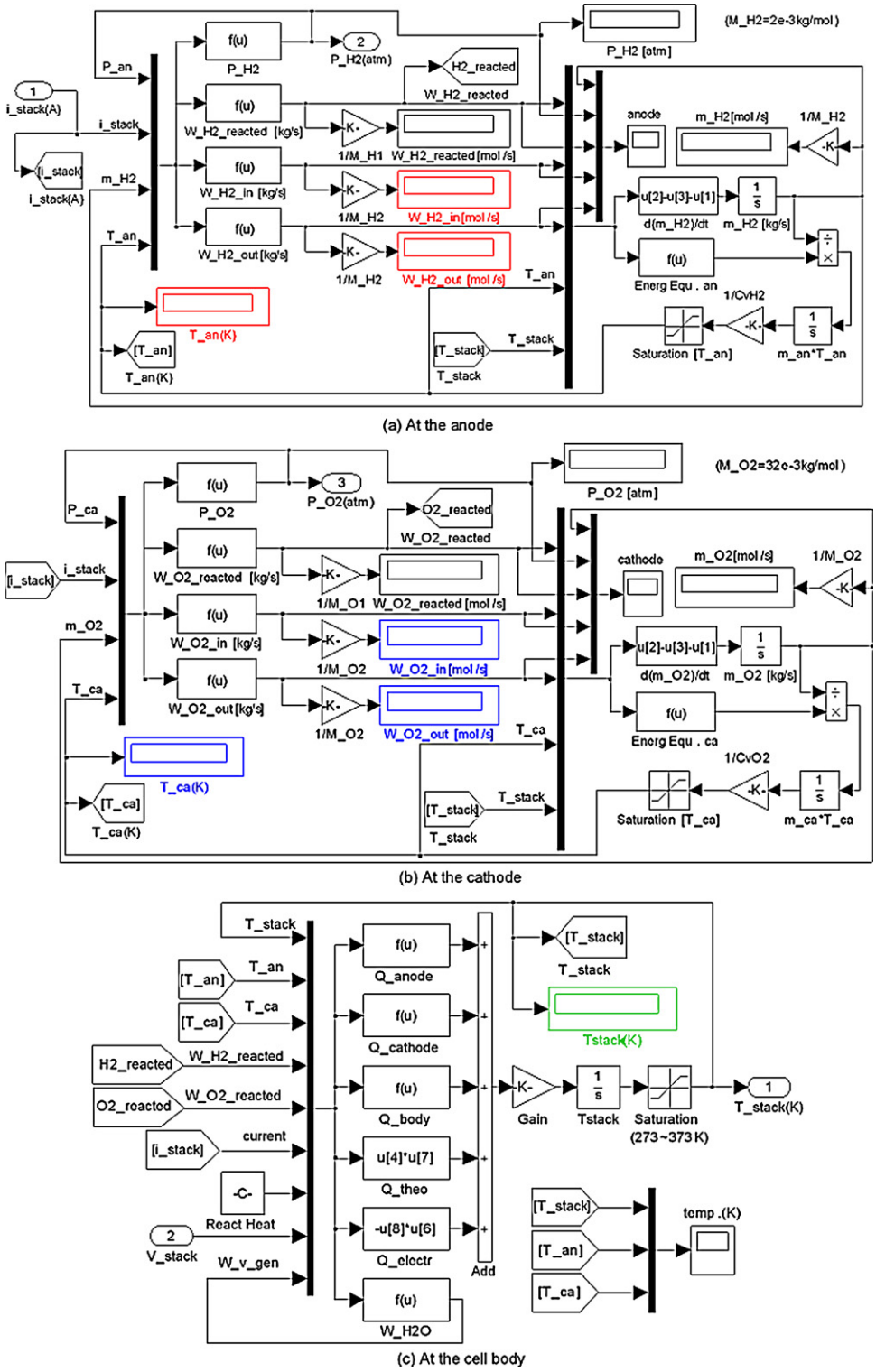

Fig. 7. SIMULINK block diagram of mass and energy transfer for the Ballard-Mark-V PEMFC.

voltage into four desired voltage levels during a load change. Generally, the converter output voltage will dip at the sudden change of load from light to heavy or jump at the sudden change of load from heavy to light. The magnitude and duration of the transient voltage occurring in the output voltages during a load change are designed to be within ±5% and 3 ms in this paper. However, the range of acceptable variation in the output voltages usually depends upon the users' applications. The output voltages and output currents for 5-, 12-, 24- and 48-V dc–dc converters during a load change are shown in Figs. 15–18, respectively. Since the output of the studied fuel cell ranges from 27 V to 40 V, only the 48-V dc–dc converter will need to use a boost-converter. The rest of converters will use buck converters. As seen from Figs. 15–18, the output voltages of four dc–dc converters all have a transient spike during a load change at 4 s. Nevertheless, their output voltages are all stable right after the load change.

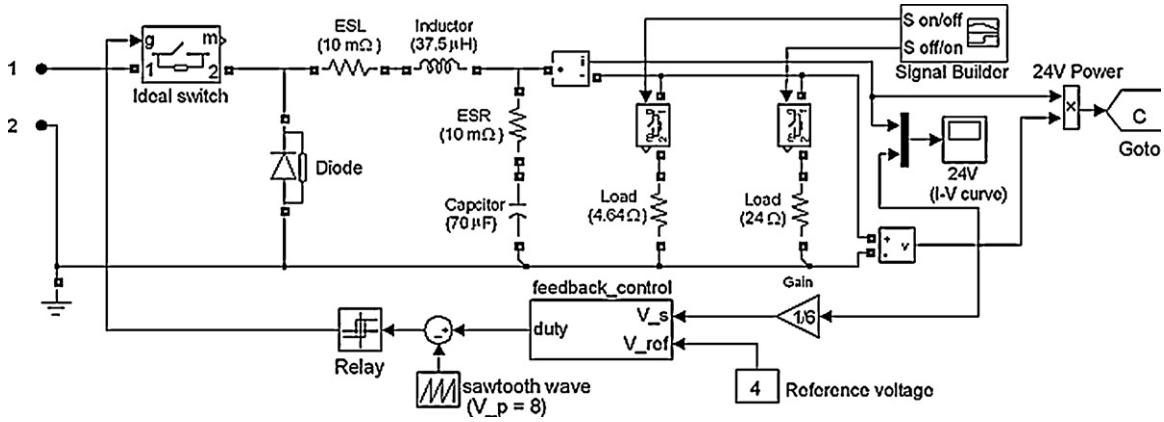

Fig. 8. SIMULINK block diagram of the converter with 24 V_{dc} output voltage.

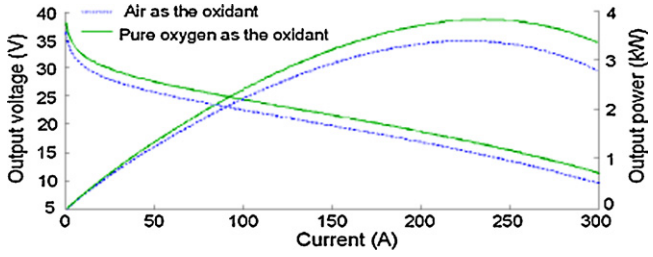

Fig. 9. Output voltage and output power of the Ballard-Mark-V PEMFC for using air or pure oxygen as the oxidant.

5.4. Simulation of the supply of the reactant gases

In this subsection, a parametric analysis to simulate transient dynamic effects on the supply of the reactant gases within the fuel cell system is carried by using the parameters listed in Table 1. Based on Table 4, the output power of the fuel cell system needs to generate about 1841 W when four converters are operated on full load condition, and it only needs about 370 W when load change from full load to light load is simultaneously occurred on four converters. The time length for the simulation is 900 s.

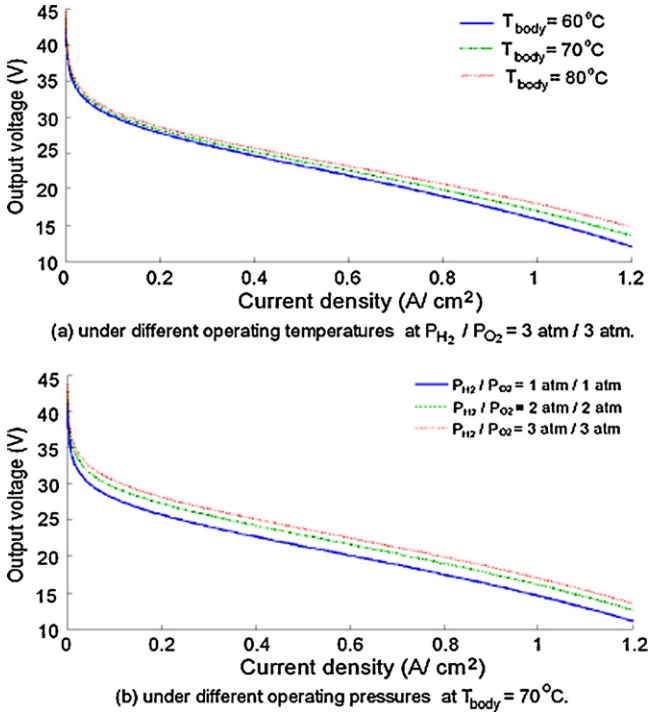

Fig. 10. Output voltage of the Ballard-Mark-V PEMFC under different operating conditions.

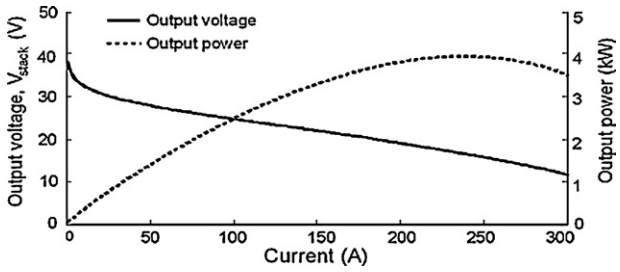

Fig. 11. Output power of the Ballard-Mark-V 35-cell 5-kW PEMFC and its corresponding output voltage.

Table 3
Voltage levels and loads for the designed AUV.

Rated voltage	Name of devices	Maximum rated power
DC 5V Bus	Embedded control main board	5 W
DC 12V Bus	Inertial measurement unit	0.78 W
	Global position system	1 W
	Pressure transducer	0.24 W
	RF modem	9 W
	CTD sensors	0.252 W
	Headlamp	100W * 3
DC 24V Bus	Ultra short baseline	10 W
	Acoustic modem	8 W
	Inertial navigation system	6 W
	Doppler velocity log	80 W
	Digit video camera	5–10 W
	Forward-looking sonar	5–10 W
DC 48V Bus	Thruster	350 W * 3
		Total about 1841 W

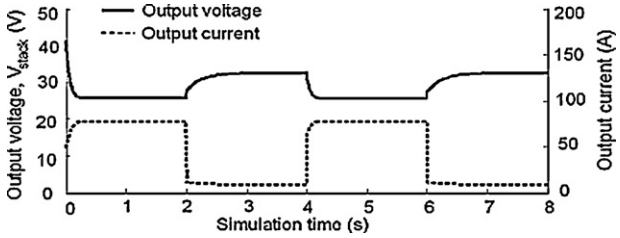

Fig. 12. Current–voltage curve of the Ballard-Mark-V 35-cell 5-kW PEMFC at the power output between 0.3 and 20 kW.

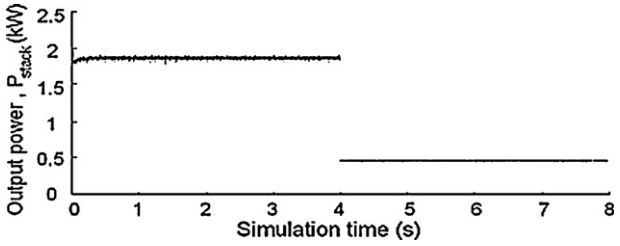

Fig. 13. Output power of the Ballard-Mark-V 35-cell 5 kW PEMFC when the load changes from full load to light load.

Fig. 19 shows the temperature histories of the stack body, anode channel and cathode channel. The temperatures of these three control volumes exhibit similar trends. During the first 300 s (i.e., at light load), the temperatures slowly increase. The reason is that the heat generated by the electrochemical reaction is more than the heat transferred to the surrounding atmosphere through convection. During the second stage (300–600 s) (i.e., load

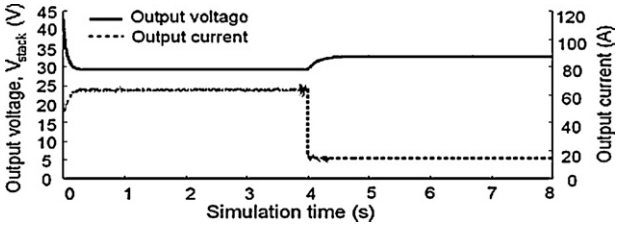

Fig. 14. Current–voltage curve of the Ballard-Mark-V 35-cell 5 kW PEMFC when the load changes from full load to light load.

Table 4
Classification of light load, full load and overload of the designed AUV at each dc bus.

Rated voltage	Light load (20%)	Full load (100%)	Overload (120%)
DC 5V	1 W	5 W	6.25 W
DC 12V	60 W	312 W	375 W
DC 24V	24 W	124 W	150 W
DC 48V	280 W	1400 W	1680 W

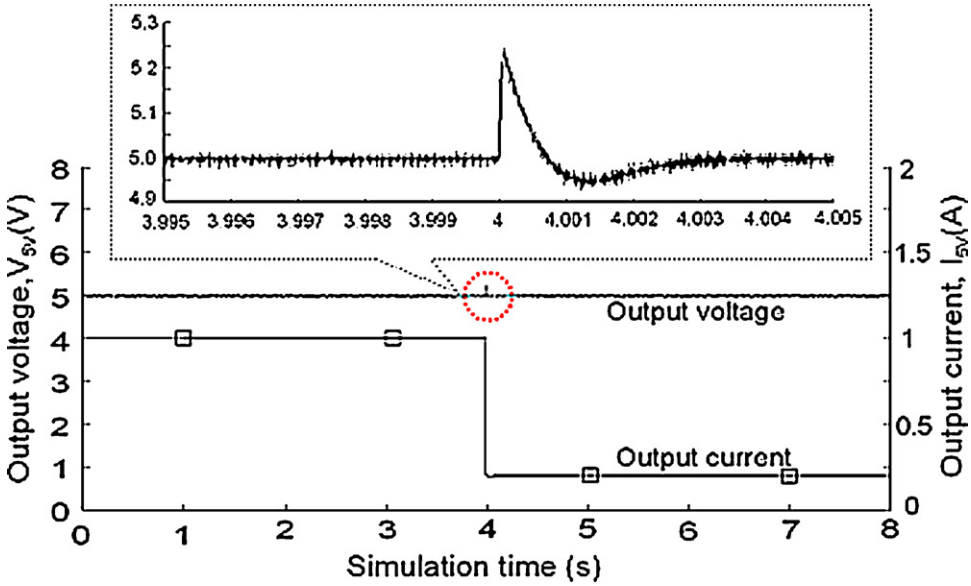

Fig. 15. Output voltage and output current of 5 V_{dc} converter during a load change from 5 Ω to 25 Ω.

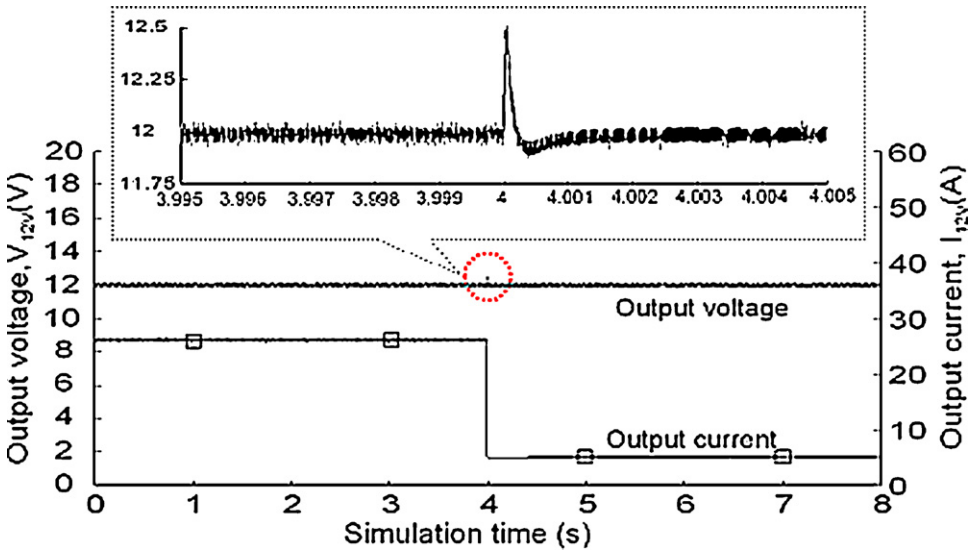

Fig. 16. Output voltage and output current of 12 V_{dc} converter during a load change from 0.46 Ω to 2.4 Ω.

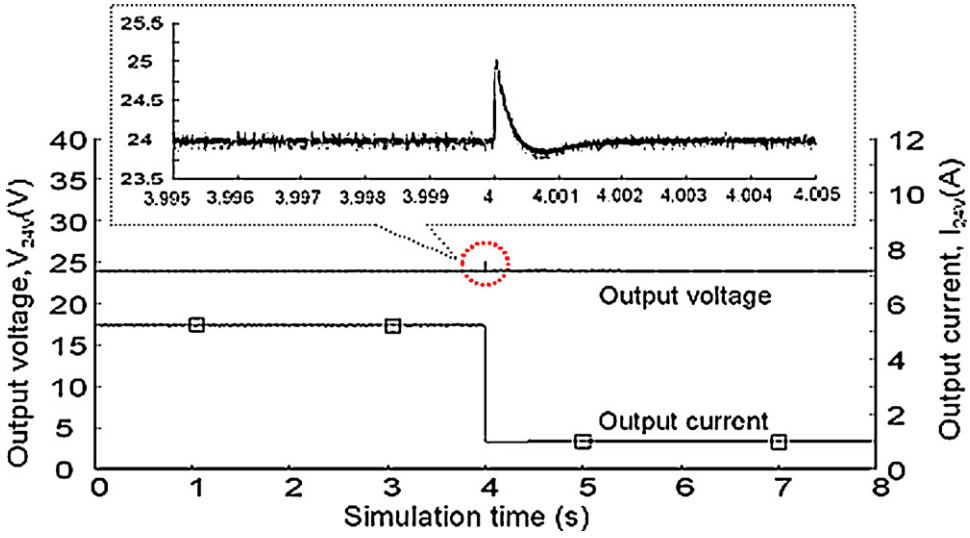

Fig. 17. Output voltage and output current of 24 V_{dc} converter during a load change from 0.46 Ω to 24 Ω.

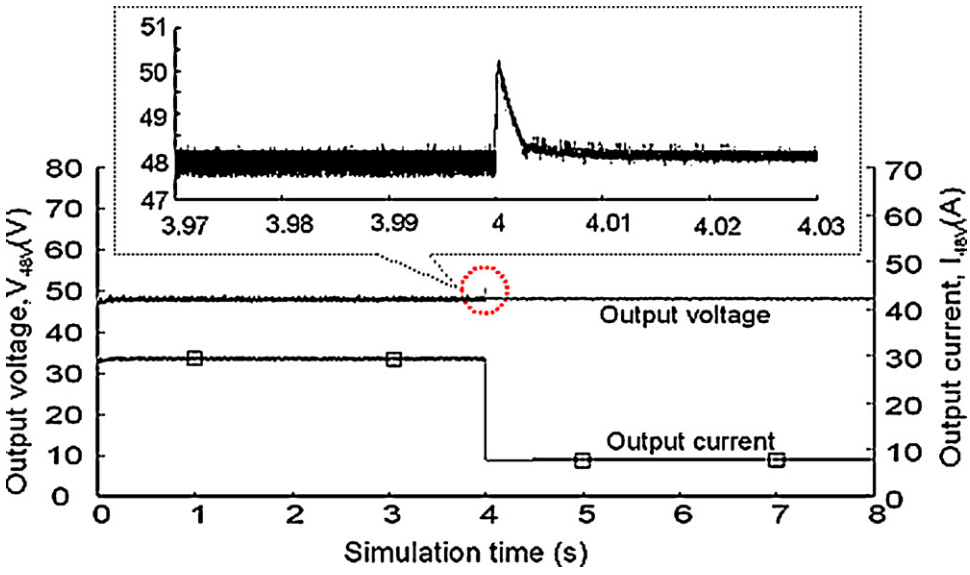

Fig. 18. Output voltage and output current of 48 V_{dc} converter during a load change from 1.46 Ω to 8.2 Ω.

change from light to full load), the output power of the stack increases due to the load current increase, and correspondingly the heat generated by the electrochemical reaction increases and overcomes the heat loss due to convection. Thus, the temperatures of stack/anode/cathode all increase. During the last stage (600–900 s) (i.e., load change from full to light load), the temperatures drop, as the output power and hence the heat generated is reduced. It is worth mentioning that the temperatures of the three control volumes differ significantly. This clearly demonstrates the advantage of dividing the fuel cell system into three control volumes.

Fig. 20 shows the pressure variation within the two channels. When the load current is high (i.e., load change from light to full load), the fuel consumed by the electrochemical reaction increases. Correspondingly, the gas pressures go down. On the contrary, when the load current is low (i.e., load change from full to light load), the pressures within the channels become relatively high. Fig. 21 shows the change of mass of gases (hydrogen, oxygen and nitrogen) within the two channels due to the load current change. During the first stage and last stage, the load current is lower, which leads to lower fuel/oxygen consumption for the electrochemical reaction and higher mass of gases within the channels. The opposite can be observed for the second stage. It is shown that hydrogen and oxygen decrease due to load current increase. This is because when the oxygen consumption increases, the pressure within the cathode channel goes down and more oxygen will enter from the inlet. The inlet mass flow rates of hydrogen and oxygen are shown in Fig. 22. Correspondingly, their

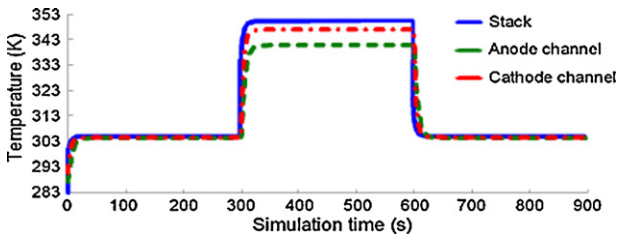

Fig. 19. Temperature change at the anode channel, cathode channel and cell body.

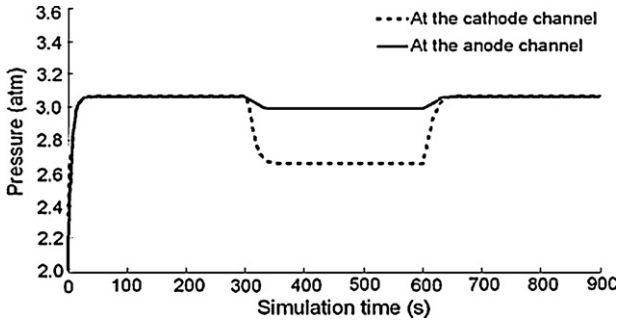

Fig. 20. Pressure change at the anode and cathode channel.

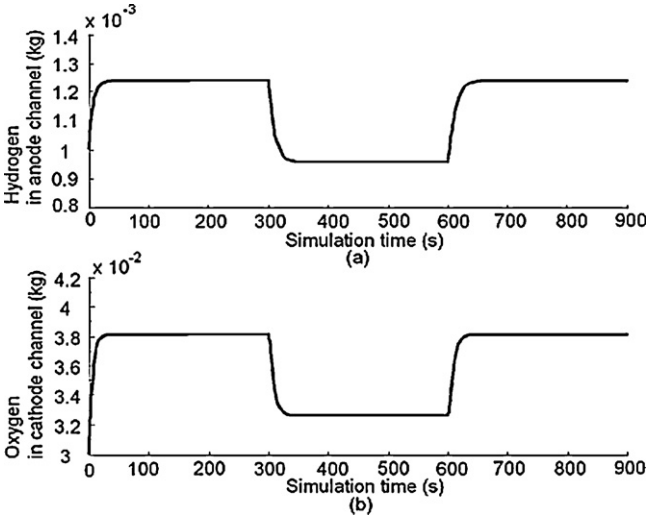

Fig. 21. Hydrogen and oxygen change within the anode and cathode channels.

mass consumptions are shown in Fig. 23. The simulation results presented here clearly illustrates the complicated dynamic interactions between temperature and gas flow, and demonstrates the necessity of developing a transient model using the control volume approach.

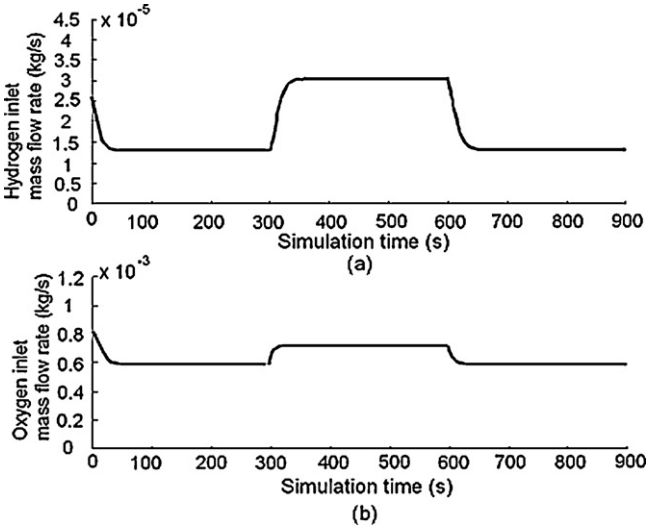

Fig. 22. Inlet mass flow rate of hydrogen and oxygen.

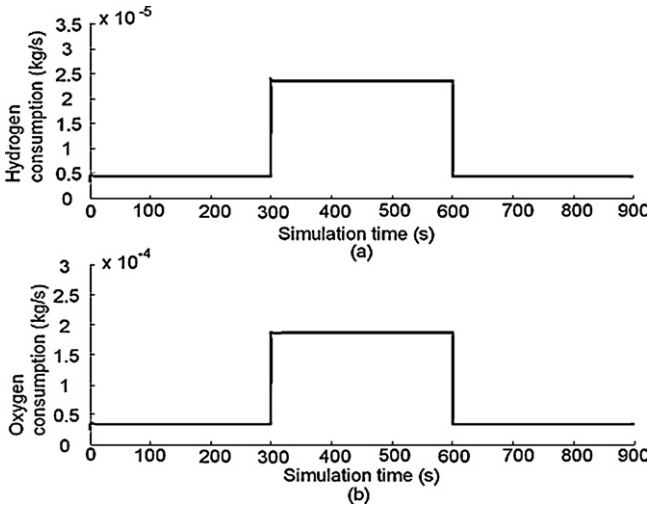

Fig. 23. Mass consumption of hydrogen and oxygen.

6. Conclusions

This paper studies the electrical behavior of Ballard-Mark-V 35-cell 5 kW PEMFC with its output voltage range from 27- to 40-V based PWM dc–dc power conversion under load changes for applications in AUVs. The models of the studied fuel cell and PWM dc–dc converters have been implemented in Matlab/SIMULINK^{TM} environment. The PEMFC model includes the double-layer charging effect, gas diffusion in the electrodes, and the thermodynamic characteristic while the operation of PWM dc–dc converter assumes to be in CCM with a compensator in voltage-mode control. A series of simulations show that the output voltages-based dc–dc power conversion with the designed compensation network is stable as the load changes from full load to light load. However, we regret that the results of the simulations have not yet been compared with actual measurements since the experimental work is in progress.

References

[1] J. Larminie, A. Dicks, Fuel Cell Systems Explained, 2nd ed., John Wiley & Sons, Inc., New York, 2003.
[2] Y. Chen, IEEE International Symposium on Underwater Technology, 2004, pp. 9–13.
[3] A.P. Meyer, Proceedings of OCEANS'93, vol. 2, Victoria, BC, Canada, October 18–21, 1993, pp. II/146-II/151.
[4] I. Yamamoto, T. Aoki, S. Tsukioka, H. Yoshida, T. Hyakudome, T. Sawa, S. Ishibashi, T. Inada, K. Yokoyama, T. Maeda, S. Ishiguro, H. Hirayama, K. Hirokawa, A. Hashimoto, N. Hisatome, T. Tani, Proceedings of OCEANS'94, vol. 3, November 9–12, 2004, pp. 1732–1737.
[5] "Autonomous Undersea Vehicle Applications Center" http://auvac.org/.
[6] P. Ray, H. Cook, Autonomous Underwater Vehicle, Senior Design Project, Stevens Institute of Technology, 2006, April.
[7] W.T. Tsai, Nonlinear circuit analysis and control of a proton exchange membrane fuel cell stack, Master Thesis, National Chung Hsing University, 2004.
[8] V.F. Pires, J. Fernando, A.A. Silva, IEEE Transactions on Education 45 (August (3)) (2002) 253–261.
[9] I. Sadli, P. Thounthong, J.-P. Martin, S. Rael, B. Davat, Journal of Power Sources 156 (May) (2006) 119–125.
[10] C. Wang, M.H. Nehrir, H. Gao, IEEE Transactions on Energy Conversion 21 (June (2)) (2006) 586–595.
[11] S.K. Mazumder, IEEE Transactions on Aerospace and Electronic Systems 42 (January (1)) (2006) 50–69.
[12] X. Xue, J. Tang, A. Smirnova, R. England, N. Sammes, Journal of Power Sources 113 (2) (2004) 188–204.
[13] P.R. Pathapati, X. Xue, J. Tang, Renewable Energy 30 (May (1)) (2004) 1–22.
[14] F.M. White, Viscous Fluid Flow, 2nd ed., McGraw-Hill, 1991.
[15] C. Wang, M.H. Nehrir, S.R. Shaw, IEEE Transactions on Energy Conversion 20 (June (2)) (2005) 442–451.
[16] J.C. Amphlett, R.M. Baumert, R.F. Mann, B.A. Peppley, P.R. Roberge, Journal of Electrochemical Society 142 (January (1)) (1995) 1–8.
[17] J.C. Amphlett, R.F. Mann, B.A. Peppley, P.R. Roberge, A. Rodrigues, Journal of Power Sources 61 (July/August (1–2)) (1996) 183–188.
[18] M.J. Khan, M.T. Iqbal, Fuel Cells (August (1)) (2004) 97–104.

[19] M.J. Khan, M.T. Iqbal, Fuel Cells (May (4)) (2005) 463–475.
[20] T.V. Nguyen, R.E. White, Journal of Electrochemical Society 140 (8) (1993) 2178–2186.
[21] A. Rowe, X. Li, Journal of Power Sources 102 (December (1)) (2001) 82–96.
[22] S.K. Mazumder, S.K. Pradhan, J. Hartvigsen, M.R. von Spakovsky, D.F. Rancruel, IEEE Transactions on Energy Conversion 22 (June (2)) (2007) 457–466.
[23] S. Pradhan, S.K. Mazumder, J. Hartvigsen, M. Hollist, ASME Journal of Fuel Cell Science and Technology May (4) (2007) 154–166.
[24] S.K. Mazumder, K. Acharya, C.L. Haynes, R. William Jr., M.R. von Spakovsky, D.J. Nelson, D.F. Rancruel, J. Hartvigsen, R.S. Gemmen, IEEE Transactions on Power Electronics 19 (5) (2004) 1263–1278.
[25] N. Mohan, Tore M. Undeland, W.P. Robbins, Power Electronics: Converters, Application, and Design, 3rd ed., Wiley, 2002, October 2002, ISBN: 978-0-471-22693-2.
[26] L. Palma, M.H. Todorovic, P. Enjeti, IEEE Transactions on Industrial Electronics 55 (March (3)) (2008) 1247–1255.
[27] B. Lau, Small-signal frequency response theory for ideal DC-to-DC converter system, Ph.D. Thesis, California Institute of Technology, September 1986.
[28] A. Khaligh, A. Emadi, IEEE Transactions on Aerospace and Electronic Systems 44 (April (2)) (2008) 766–782.
[29] S. Moisseev, K. Soshin, M. Nakaoka, IEEE Transactions on Aerospace and Electronic Systems 41 (January (1)) (2005) 174–180.
[30] H. Li, F.Z. Peng, IEEE Transactions on Aerospace and Electronic Systems 40 (January (1)) (2004) 272–283.
[31] J.H. Su, C.M. Wang, J.J. Chen, J.D. Lee, T.L. Chen, IEEE PEDS (2005) 1256–1261.
[32] S.-Y. Choe, J.-W. Ahn, J.-G. Lee, S.-H. Baek, IEEE Transactions on Energy Conversion 23 (June (2)) (2008) 669–680.